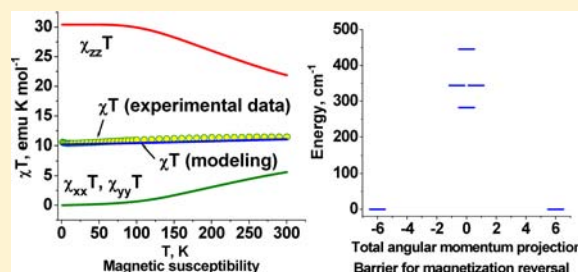


A Model of Magnetic and Relaxation Properties of the Mononuclear $[Pc_2Tb]^-TBA^+$ ComplexO. S. Reu, A. V. Palii, S. M. Ostrovsky, P. L. W. Tregenna-Piggott,[†] and S. I. Klokishner*

Institute of Applied Physics, Academy of Sciences of Moldova, Academy str. 5, Kishinev, MD-2028, Moldova

Supporting Information

ABSTRACT: The present work is aimed at the elaboration of the model of magnetic properties and magnetic relaxation in the mononuclear $[Pc_2Tb]^-TBA^+$ complex that displays single-molecule magnet properties. We calculate the Stark structure of the ground 7F_6 term of the Tb^{3+} ion in the exchange charge model of the crystal field, taking account for covalence effects. The ground Stark level of the complex possesses the maximum value of the total angular momentum projection, while the energies of the excited Stark levels increase with decreasing $|M_J|$ values, thus giving rise to a barrier for the reversal of magnetization. The one-phonon transitions between the Stark levels of the Tb^{3+} ion induced by electron-vibrational interaction are shown to lead to magnetization relaxation in the $[Pc_2Tb]^-TBA^+$ complex. The rates of all possible transitions between the low-lying Stark levels are calculated in the temperature range $14\text{ K} < T < 40\text{ K}$. With the purpose of calculation of the temperature dependence of the relaxation time of magnetization, we solve the set of master equations for the populations of the Stark levels. The relaxation time is shown to diminish from 3.2×10^{-2} s to 1.52×10^{-4} s as the temperature increases from 27 K to 40 K. The obtained values of the relaxation time are in satisfactory agreement with the observed ones. The developed model also provides satisfactory description of the dc-magnetic data and paramagnetic shifts.



1. INTRODUCTION

Because of nanometric size, quantum effects in the magnetic properties, and extremely long magnetic relaxation times, single-molecule magnets (SMMs)¹ have been considered as promising candidates for the development of high-density magnetic memories, molecular spintronic applications,² and quantum computing devices.³ The majority of known SMMs contains transition-metal ions with orbitally nondegenerate ground states (spin clusters). The Mn_{12} cluster derivatives $[Mn_{12}O_{12}(O_2CR)_{16}(H_2O)_x]^{n-}$ ($n = 0, 1, 2; x = 3, 4$),^{4–12} distorted cubane complexes with $[M^IVM^{III}_4O_3X]$ cores,^{13–15} tetranuclear vanadium complexes $[V_4O_2(O_2CR)_7(L)_2]^{n,16}$ and iron complexes¹⁷ $[Fe_8O_2(OH)_{12}(L)_6]^{8+}$ exemplify this type of SMMs. The exchange interaction couples the spins of individual ions in these clusters and promotes the appearance of the ground state with a large spin S . Thus, the energy barrier for magnetization reversal in spin clusters appears as a result of the combination of a large ground-state spin S of the cluster and a negative zero-field splitting parameter D_S . Particularly, the increase of the full spin S seemed to be a promising way to design SMMs with higher blocking temperatures. However, as has been recently demonstrated,¹⁸ the zero-field splitting parameter D_S proves to be proportional to S^{-2} and, hence, the barrier $\Delta_b = D_S S^2$ does not rise with the increase of S . Probably for this conceptually important reason, the attempts to increase S by the synthesis of big spin clusters with high values of the ground state spin have not yet produced better SMMs. As a result, the relaxation of magnetization in existing

transition-metal clusters with SMM properties is still very fast. For instance, for the $Mn_{12}Ac^{4.5}$ cluster having a barrier of ~ 61 K, the relaxation time at $T = 2$ K is 3.7×10^6 s (1.5 month). Meanwhile, the relaxation time acceptable for applications should be at least 4.7×10^8 s (15 years) at room temperature.

In an attempt to increase both the energy barrier for magnetization reversal and the lifetime of magnetization, researchers have turned to SMMs that contain transition-metal ions with unquenched orbital angular momenta in the ground state.^{19–22} We demonstrated^{23–28} that, for SMMs of this type, the first-order single-ion anisotropy and the anisotropy of exchange interaction are responsible for the formation of the barrier for magnetization reversal. At the same time, the presence of unquenched orbital angular momenta plays an ambivalent role. On the one hand, it gives rise to the magnetic anisotropy that is much stronger than in spin clusters. From the other hand, transition-metal ions with orbitally degenerate ground states strongly interact with different symmetry vibrations of the nearest ligand surrounding and also show slow relaxation of magnetization in a narrow temperature range.

Considerable effort has been focused on the design of SMMs functioning at higher temperatures than those demonstrated by SMMs based on transition-metal ions. In refs 29–32, a new class of SMMs, comprised of lanthanide ions, has been

Received: June 29, 2012

Published: September 26, 2012

reported. This class is represented by three phthalocyanine double-decker mononuclear complexes $[Pc_2Ln]^-TBA^+$ (Pc = dianion of phthalocyanine, $TBA^+ = N(C_4H_9)_4^+$, $Ln = Tb, Dy, Ho$) containing trivalent lanthanide ions. Later, it was shown that polyoxometalates encapsulating lanthanides with coordination geometries similar to those in phthalocyanides can also exhibit SMM behavior.^{33,34} In ref 35, a new heteroleptic bis(phthalocyaninato) terbium(III) complex, bearing a pyrenyl group, was shown to exhibit temperature and frequency dependence of ac magnetic susceptibility, typical of SMMs. The attachment of this complex to single-walled carbon nanotubes (SWCNTs) using π - π interactions yielded a SMM-SWCNT magnetic conjugate that demonstrates improved SMM behavior. An original supramolecular spin valve consisting of $TbPc_2$ SMMs and SWCNT components has been presented in ref 36. Upon reversing the magnetic field, the device exhibits magnetoresistance ratios up to 300% at temperatures less than 1 K. These results open up prospects for new spintronic devices with quantum properties. Electronic transport studies on a $TbPc_2$ SMM in a transistor-like setup, taking measurements of a single nuclear spin have been performed in ref 37. It was predicted that the observed long lifetimes (tens of seconds) and relaxation characteristics of nuclear spin at the single-atom scale may give rise to a completely new world of devices in which quantum logic may be implemented.

The magnetic properties of mononuclear lanthanide magnets^{29–34} are determined both by the total angular momentum J of the ground state and the strength of the axial crystal field. In these magnets, the ground state with a high value of the total angular momentum projection $|M_J|$ is generated for a single ion, because of the strong magnetic anisotropy easily derived from the 4f-component. Actually, the single-ion anisotropy of 4f ions is usually much stronger, compared with those exhibiting by 3d, 4d, and 5d ions. One more advantage of the mononuclear lanthanide-based complexes is the possibility to improve their SMM properties drastically by controlling the Stark structure of the ground multiplet with the aid of the proper change of the nearest ligand surrounding.

The interaction of lanthanide ions with the vibrations of the ligand surrounding is much weaker than that for transition-metal ions and, consequently, the relaxation is much slower in lanthanide-based SMMs, compared to those based on transition-metal ions. In fact, mononuclear lanthanide complexes demonstrate slow magnetization relaxation in temperature ranges significantly higher than those of previously known transition-metal SMMs. Thus, the $[Pc_2Ln]^-TBA^+$ and $[Pc_2Dy]^-TBA^+$ complexes exhibit out-of-phase ac susceptibility χ''_M peaks at 40 and 10 K with a 10^3 Hz ac field, respectively, while there has been no report on polynuclear transition-metal complexes with a χ''_M peak temperature higher than 7 K.

At the same time, neither fluorescence nor absorption spectra associated with lanthanide centers are obtainable in phthalocyanine double-decker complexes, because of the low-lying Pc -centered energy levels quenching the lanthanide fluorescence, and the extremely intense Pc -centered absorption bands concealing the lanthanide-centered bands. Therefore, the theoretical analysis of binuclear and mononuclear lanthanide phthalocyanine complexes performed in refs 29–32, 38, and 39 is limited to the determination of the Stark structure of lanthanide ions, using NMR paramagnetic shifts and magnetic susceptibility data, instead of f-f spectroscopic ones. In the

approach suggested in refs 29–32, 38, and 39, the set of ligand field parameters that gives the least-squares fit to the experimental data is determined under the restriction that each parameter represents a linear function of the number of f-electrons in the lanthanide ion. Such an assumption is not quite justified and actually leads to 10 fitting parameters in the crystal field model for $[Pc_2Ln]^-TBA^+$. Thus, the problem of microscopic calculation of the energy spectrum of lanthanides in $[Pc_2Ln]^-TBA^+$ complexes requires special consideration. The microscopic calculation of the Stark structure of lanthanides will give the possibility to model the magnetic and relaxation properties.

In ref 30, the first attempt was made to understand the mechanism of magnetic relaxation in lanthanide-based SMMs qualitatively, examining the temperature dependence of the relaxation time τ extracted from the χ'' component of the ac susceptibility. The experimental study and semiempirical interpretation of the electron spin dynamics in the anionic form of the bis-phthalocyaninato terbium(III) molecule $[Pc_2Ln]^-TBA^+$ has been addressed in ref 40 by means of solid-state 1H NMR spectroscopy. For the $[Pc_2Tb]^-TBA^+$ complex in ref 30, the observed values of τ in the temperature range of 25–40 K were fitted to those corresponding to the two-phonon Orbach process, while at temperatures below 25 K, the direct or Raman process was supposed to be the determinative one in relaxation. In fact, the semiempirical analysis performed in ref 30 does not allow one to distinguish between the contributions of the direct, Orbach, and Raman processes to magnetization relaxation. However, it is well-known that, for lanthanide ions, the contribution of direct one-phonon transitions is dominating and should be taken into account^{27,41–44} in the first place. Therefore, in the present work, we are going to address the problem of relaxation in the $[Pc_2Ln]^-TBA^+$ complexes and, at first stage, to evaluate microscopically the values of the relaxation time taking into account only the one-phonon processes.^{27,41–44}

Summarizing the aforementioned introduction, it should be mentioned that the articles dealing with 4f SMMs^{29–34} do not contain comprehensive theoretical models that are able to explain the observed SMM behavior of these systems. Meanwhile, the accurate theoretical description of the 4f SMMs requires a crystal field model, taking into account the structural lattice parameters and the point charges of the ligands, as well as the covalence of the lanthanide–ligand bond. No less important is the examination of the interaction between the localized 4f electrons and lattice vibrations and establishing the role of this interaction in magnetization relaxation. Thus, the goal of the present article is to develop a model for explanation of the strong magnetic anisotropy and slow relaxation of magnetization exhibited by $[Pc_2Ln]^-TBA^+$ complexes demonstrating SMM properties. On the basis of this model, the temperature dependence of the magnetic susceptibility and relaxation time for the $[Pc_2Ln]^-TBA^+$ complex will be calculated and compared with experimental ones.

2. THE MODEL

2.1. Crystal-Field Operator for the Tb^{3+} Ion. For strongly screened f-electrons of lanthanide ions, a sufficiently adequate approximation is the allowance for the interaction with the ions of the nearest surrounding. The nearest local environment of the Tb^{3+} ion in the $[Pc_2Ln]^-TBA^+$ compound consists of eight N atoms. Their spherical coordinates, with

Table 1. Ligand Positions

real symmetry	1	2	3	4	5	6	7	8
R (Å)	2.44	2.44	2.44	2.44	2.43	2.43	2.43	2.43
θ (°)	126.5	126.5	126.5	126.5	53.8	53.8	53.8	53.8
φ (°)	34.5	124.5	214.5	304.5	0	90	180	270

respect to the central Tb^{3+} ion⁴⁵ placed at the origin of spherical coordinate system, are given in Table 1. From this data,⁴⁵ it is seen that the skew angle made by the two Pc rings is 34.5° , and the real site symmetry of the Tb^{3+} ion is C_4 .

In this case, the crystal field Hamiltonian acting within the space of the $4f$ orbitals of the lanthanide ion can be written in the following form:

$$H_{cf} = A_2^0 C_2^0 + A_4^0 C_4^0 + A_4^4 (C_4^4 + C_4^{-4}) + B_4^4 (C_4^{-4} - C_4^4) + A_6^0 C_6^0 + A_6^4 (C_6^4 + C_6^{-4}) + B_6^4 (C_6^{-4} - C_6^4) \quad (1)$$

where A_p^m and B_p^m are the crystal field parameters, $C_p^m(\vartheta, \varphi) = [4\pi/(2p+1)]^{1/2} Y_p^m(\vartheta, \varphi)$ are the tensor spherical operators ($Y_p^m(\vartheta, \varphi)$ are the normalized spherical harmonics).

The crystal field parameters can be evaluated in the framework of the exchange-charge model^{46–54} that takes into account two contributions to the energy of the $4f$ valent electrons in the crystal field, namely, the contribution arising from the interaction of the $4f$ electrons with the point charges (pc) of the surrounding ligands and the contribution coming from the overlap of the $4f$ orbitals with the ligand orbitals. The latter is referred to as the contribution of exchange charges (ec). In the exchange-charge model of the crystal field the parameters A_p^{lml} and B_p^{lml} are represented as

$$A_p^{lml} = A_p^{lml(pc)} + A_p^{lml(ec)}, \quad B_p^{lml} = B_p^{lml(pc)} + B_p^{lml(ec)} \quad (2)$$

The components $A_p^{lml(pc)}$ and $B_p^{lml(pc)}$ are usually determined as follows:^{46–54}

$$A_p^{lml(pc)} = (-1)^m \sum_{\alpha} \frac{Z_{\alpha} e^2 \langle r^p \rangle (1 - \sigma_p)}{2(R_{\alpha})^{p+1}} \times [C_p^m(\vartheta_{\alpha}, \varphi_{\alpha}) + C_p^{m*}(\vartheta_{\alpha}, \varphi_{\alpha})] \\ B_p^{lml(pc)} = (-1)^m \sum_{\alpha} \frac{Z_{\alpha} e^2 \langle r^p \rangle (1 - \sigma_p)}{2(R_{\alpha})^{p+1}} \times [C_p^m(\vartheta_{\alpha}, \varphi_{\alpha}) - C_p^{m*}(\vartheta_{\alpha}, \varphi_{\alpha})] \quad (3)$$

where $Z_{\alpha} e$ is the effective charge of ligand α with the spherical coordinates $R_{\alpha}, \vartheta_{\alpha}, \varphi_{\alpha}$, $\langle r^p \rangle$ is the radial integral for the Tb^{3+} ion, σ_p is the shielding factor. In the subsequent calculations, the values $\langle r^2 \rangle = 0.893$ au, $\langle r^4 \rangle = 2.163$ au, $\langle r^6 \rangle = 11.75$ au, and $\sigma_2 = 0.523$, $\sigma_4 = -0.0107$, $\sigma_6 = -0.0318$ ⁵⁵ have been used.

The parameters $A_p^{lml(ec)}$ and $B_p^{lml(ec)}$ are given by the following relations:^{46–54}

$$A_p^{lml(ec)} = (-1)^m \frac{e^2(2p+1)}{R_{\alpha}^7} \times \sum_{\alpha} \frac{S_p(R_{\alpha})}{R_{\alpha}} [C_p^m(\vartheta_{\alpha}, \varphi_{\alpha}) + C_p^{m*}(\vartheta_{\alpha}, \varphi_{\alpha})] \\ B_p^{lml(ec)} = (-1)^m \frac{e^2(2p+1)}{R_{\alpha}^7} \times \sum_{\alpha} \frac{S_p(R_{\alpha})}{R_{\alpha}} [C_p^m(\vartheta_{\alpha}, \varphi_{\alpha}) - C_p^{m*}(\vartheta_{\alpha}, \varphi_{\alpha})] \quad (4)$$

where $S_p(R_{\alpha})$ are the overlap integrals, determined as

$$S_p(R_{\alpha}) = G_s S_s^2(R_{\alpha}) + G_{\sigma} S_{\sigma}^2(R_{\alpha}) + \gamma_p G_{\pi} S_{\pi}^2(R_{\alpha}), \\ \gamma_2 = \frac{3}{2}, \quad \gamma_4 = \frac{1}{3}, \quad \gamma_6 = -\frac{3}{2} \quad (5)$$

where the values G_s , G_{σ} and G_{π} are the dimensionless phenomenological parameters of the model, and $S_s(R_{\alpha})$, $S_{\sigma}(R_{\alpha})$, $S_{\pi}(R_{\alpha})$ are the overlap integrals of the $4f$ wave functions of the Tb^{3+} ion with $2s$, $2p$ wave functions of the nitrogen atom ($S_s(R_{\alpha}) = \langle 4f, m=0 | 2s \rangle$, $S_{\sigma}(R_{\alpha}) = \langle 4f, m=0 | 2p, m=0 \rangle$, $S_{\pi}(R_{\alpha}) = \langle 4f, m=1 | 2p, m=1 \rangle$). Numerical values of the overlap integrals have been computed with the aid of the radial $4f$ wave functions of Tb^{3+} and $2s$, $2p$ functions of N given in refs 56 and 57.

We then record the crystal field potential (eq 1), in terms of equivalent operators:⁵⁸

$$H_{cf} = a_2^0 O_2^0 + a_4^0 O_4^0 + a_6^0 O_6^0 + a_4^4 O_4^4 + b_4^4 Q_4^4 + a_6^4 O_6^4 + b_6^4 Q_6^4 \quad (6)$$

where the parameters a_l^m and b_l^m are associated with the parameters A_l^m and B_l^m of the Hamiltonian H_{cf} (eq 1) by the relations

$$a_l^0 = A_l^0 \gamma_{l0} \langle J \| \xi_l \| J \rangle \sqrt{\frac{4\pi}{2l+1}} \\ a_l^m = A_l^m \gamma_{lm} \langle J \| \xi_l \| J \rangle \sqrt{\frac{4\pi}{2l+1}} \\ b_l^m = B_l^m \gamma_{lm} \langle J \| \xi_l \| J \rangle \sqrt{\frac{4\pi}{2l+1}} \quad (7)$$

Here, the parameters $\langle J \| \xi_l \| J \rangle$ ($l = 2, 4, 6$) are the so-called Stevens constants α , β , γ , which take on the values $\alpha = -1/(3^2 \times 11)$, $\beta = 2/(3^3 \times 5 \times 11^2)$ and $\gamma = -1/(3^4 \times 7 \times 11^2 \times 13)$.⁵⁹ The expressions of the crystal field parameters a_{lm} , b_{lm} as functions of G_s , G_{σ} and G_{π} and the numerical values of the constants γ_{lm} are given in Appendix A.

2.2. Electron–Phonon Interaction. Probabilities of One-Phonon Transitions. The evaluation of the probabilities of nonradiative transitions that facilitate magnetic relaxation requires a model of electron–phonon interaction Hamiltonian and phonon dispersion law. Therefore, later in this paper, in correspondence with the real experimental situation, we consider a crystal consisting of noninteracting $[\text{Pc}_2\text{Tb}]^{-}\text{TBA}^{+}$

complexes. For lanthanide ions, being an example of a small-radius center, the Hamiltonian of electron–phonon interaction is based on the ligand-field theory. In the above employed quasi-molecular (cluster) model that considers the lanthanide ion as a complex formed by the central ion and the adjacent ions of the lattice the displacements of the ligands are assumed to appear because of modulation of the crystal field by lattice vibrations. The operator H_{eL} of electron–vibrational interaction consists of parts corresponding to the irreducible vibrational representations $\bar{\Gamma}$ of the point group of the Tb center^{42,60}

$$H_{eL} = \sum_{\bar{\mu}\bar{\Gamma}\bar{\gamma}} V_{\bar{\mu}\bar{\Gamma}\bar{\gamma}} Q_{\bar{\mu}\bar{\Gamma}\bar{\gamma}} \quad (8)$$

Here, $\bar{\gamma}$ is the row index of $\bar{\Gamma}$, $\bar{\mu}$ enumerates the repeating vibrational representations, $Q_{\bar{\mu}\bar{\Gamma}\bar{\gamma}}$ are the symmetrical displacements of the complex, $V_{\bar{\mu}\bar{\Gamma}\bar{\gamma}}$ are the irreducible tensor operators, which transform according to the $\bar{\Gamma}$ -representation. The operators $V_{\bar{\mu}\bar{\Gamma}\bar{\gamma}}$ (possessing the dimension of energy) can be expressed as derivatives of the potential energy $W(\mathbf{r}_i - \mathbf{R}_\alpha)$ of the interaction of the electrons of the Tb³⁺ ion and the nitrogen ligands:

$$V_{\bar{\mu}\bar{\Gamma}\bar{\gamma}}(\mathbf{r}) = \sum_{\alpha,i} \left. \frac{\partial W(\mathbf{r}_i - \mathbf{R}_\alpha)}{\partial Q_{\bar{\mu}\bar{\Gamma}\bar{\gamma}}} \right|_{Q_{\bar{\mu}\bar{\Gamma}\bar{\gamma}}=0} \quad (9)$$

The operators $V_{\bar{\mu}\bar{\Gamma}\bar{\gamma}}$ for the complex formed by the Tb³⁺ ion and its nearest surrounding can be obtained by substitution of the crystal field potential (eqs 1–3) at arbitrary \mathbf{R}_α into eq 9 with the subsequent differentiation of the parameters $A_p^{lm(pc)}$, $A_p^{lm(ec)}$ and $B_p^{lm(pc)}$, $B_p^{lm(ec)}$ over the projections of the position vectors \mathbf{R}_α of the ligands. Just like the overlap integrals $S_p(R)$, their derivatives $S'_p(R)$, which are necessary to obtain the operators $V_{\bar{\mu}\bar{\Gamma}\bar{\gamma}}$ can be calculated with the aid of the radial wave functions of terbium and nitrogen, given in refs 56 and 57.

The Hamiltonian of electron–phonon interaction is taken in the form

$$H_{eL} = \sum_{\kappa\eta} (V_{\kappa\eta} a_{\kappa\eta}^+ + V_{\kappa\eta}^* a_{\kappa\eta}) \quad (10)$$

where $a_{\kappa\eta}^+$ ($a_{\kappa\eta}$) is the creation (annihilation) operator of the phonon having the wave vector κ and the index of the vibration branch η . The operators $V_{\kappa\eta}$ are associated with the operators $V_{\bar{\mu}\bar{\Gamma}\bar{\gamma}}(\mathbf{r})$ by the relation^{43,44}

$$V_{\kappa\eta} = \sum_{\bar{\mu}\bar{\Gamma}\bar{\gamma}} \left(\frac{\hbar}{2NM_0\omega_{\kappa\eta}} \right)^{1/2} V_{\bar{\mu}\bar{\Gamma}\bar{\gamma}} f_{\bar{\mu}\bar{\Gamma}\bar{\gamma}}(\kappa\eta) \quad (11)$$

where N is the number of unit cells in the crystal, M_0 is the mass of the nitrogen ligand, the coefficients $f_{\bar{\mu}\bar{\Gamma}\bar{\gamma}}(\kappa\eta)$ perform the transformation from the symmetric displacements $Q_{\bar{\mu}\bar{\Gamma}\bar{\gamma}}$ to the normal modes of the crystal.

Furthermore, we assume that one-phonon transitions are responsible for the relaxation of magnetization in the system under examination. The probability of one-phonon transition between the states $|\bar{\Gamma}\bar{\gamma}\rangle$ and $|\Gamma\gamma\rangle$ of the Tb complex is given by the relation^{27,41–44}

$$W_{\bar{\Gamma}\bar{\gamma} \rightarrow \Gamma\gamma} = \frac{2\pi}{\hbar^2} \sum_{\kappa,\eta} |\langle \Gamma\gamma | V_{\kappa\eta} | \bar{\Gamma}\bar{\gamma} \rangle|^2 \left\{ \begin{array}{l} \bar{n}(\omega_{\kappa\eta}) \\ \bar{n}(\omega_{\kappa\eta}) + 1 \end{array} \right\} \times \delta(\omega_{\kappa\eta} - |\Delta_{\Gamma\gamma, \bar{\Gamma}\bar{\gamma}}|) \quad (12)$$

where the phonon occupation numbers are given as

$$\bar{n}(\omega_{\kappa\eta}) = \frac{1}{\exp\left(\frac{\hbar\omega_{\kappa\eta}}{kT}\right) - 1} \quad (13)$$

In the process with one-phonon absorption, the probability $W_{\bar{\Gamma}\bar{\gamma} \rightarrow \Gamma\gamma}$ is proportional to $\bar{n}(|\Delta_{\Gamma\gamma, \bar{\Gamma}\bar{\gamma}}|)$; when one phonon is emitted, $W_{\bar{\Gamma}\bar{\gamma} \rightarrow \Gamma\gamma} \approx \bar{n}(|\Delta_{\Gamma\gamma, \bar{\Gamma}\bar{\gamma}}|) + 1$.

With the aid of eq 11 and transformations described in refs 43 and 44, one can present eq 12 in the following form:

$$W_{\bar{\Gamma}\bar{\gamma} \rightarrow \Gamma\gamma} = \frac{\pi}{NM_0\hbar} \sum_{\kappa,\eta} \sum_{\bar{\mu}, \bar{\mu}'} \frac{1}{[\bar{\Gamma}]\omega_{\kappa\eta}} \langle \Gamma\gamma | V_{\bar{\mu}\bar{\Gamma}\bar{\gamma}} | \bar{\Gamma}\bar{\gamma} \rangle^* \langle \Gamma\gamma | V_{\bar{\mu}'\bar{\Gamma}\bar{\gamma}} | \bar{\Gamma}\bar{\gamma} \rangle \times \sum_{\gamma} f_{\bar{\mu}\bar{\Gamma}\bar{\gamma}}^*(\kappa\eta) f_{\bar{\mu}'\bar{\Gamma}\bar{\gamma}}(\kappa\eta) \left\{ \begin{array}{l} \bar{n}(\hbar\omega_{\kappa\eta}) \\ \bar{n}(\hbar\omega_{\kappa\eta}) + 1 \end{array} \right\} \times \delta(\omega_{\kappa\eta} - |\Delta_{\Gamma\gamma, \bar{\Gamma}\bar{\gamma}}|) \quad (14)$$

At low temperatures, which are actual for the problem under consideration, only acoustic vibrational modes are excited in the crystal. For consideration of these modes, we employ the Debye model in which the phonon frequencies are independent of the direction of the wave vector κ and obey the dispersion law $\omega_{\kappa\eta} = \kappa v_{\text{eff}}$. Here, v_{eff} is the effective speed of sound in the crystal. Replacing in eq 14, the summation over κ by integration, with the aid of the relations

$$\int d\Omega_{\kappa} \sum_{\gamma} f_{\bar{\mu}\bar{\Gamma}\bar{\gamma}}^*(\kappa\eta) f_{\bar{\mu}'\bar{\Gamma}\bar{\gamma}}(\kappa\eta) = \frac{4\pi M_0 [\bar{\Gamma}]}{M} \varphi_{\bar{\mu}\bar{\mu}'\bar{\Gamma}}(\kappa) \quad (15)$$

$$\varphi_{\bar{\mu}\bar{\mu}'\bar{\Gamma}}(\kappa) = \delta_{\bar{\mu}\bar{\mu}'} + \sum_{\alpha \neq \alpha'} (U_{\alpha}^{\bar{\mu}\bar{\Gamma}\bar{\gamma}})^* U_{\alpha}^{\bar{\mu}'\bar{\Gamma}\bar{\gamma}} \frac{\sin(\kappa|\mathbf{R}_{\alpha}^0 - \mathbf{R}_{\alpha'}^0|)}{\kappa|\mathbf{R}_{\alpha}^0 - \mathbf{R}_{\alpha'}^0|} \quad (16)$$

one can present eq 14 in the following form:

$$W_{\bar{\Gamma}\bar{\gamma} \rightarrow \Gamma\gamma} = \frac{|\Delta_{\Gamma\gamma, \bar{\Gamma}\bar{\gamma}}|}{2\pi\rho\hbar v_{\text{eff}}^3} \sum_{\bar{\mu}, \bar{\mu}'} \varphi_{\bar{\mu}\bar{\mu}'\bar{\Gamma}} \left(\frac{|\Delta_{\Gamma\gamma, \bar{\Gamma}\bar{\gamma}}|}{v_{\text{eff}}} \right) \langle \Gamma\gamma | V_{\bar{\mu}\bar{\Gamma}\bar{\gamma}} | \bar{\Gamma}\bar{\gamma} \rangle^* \times \langle \Gamma\gamma | V_{\bar{\mu}'\bar{\Gamma}\bar{\gamma}} | \bar{\Gamma}\bar{\gamma} \rangle \left\{ \begin{array}{l} \bar{n}(|\Delta_{\Gamma\gamma, \bar{\Gamma}\bar{\gamma}}|) \\ \bar{n}(|\Delta_{\Gamma\gamma, \bar{\Gamma}\bar{\gamma}}|) + 1 \end{array} \right\} \quad (17)$$

where M is the mass of the unit cell, ρ is the density of the crystal, and $U_{\alpha}^{\bar{\mu}\bar{\Gamma}\bar{\gamma}}$ is the unitary matrix^{43,44} for the transformation of the Cartesian displacements $\Delta\mathbf{R}_{\alpha}$ of the ligands into the symmetrical coordinates $Q_{\bar{\mu}\bar{\Gamma}\bar{\gamma}}$ of the complex (see Appendix B).

2.3. Calculation of the Magnetic Properties and Paramagnetic Shifts. With the aid of eqs 1–4, we perform the calculation of the parameters of the operator of the crystal field acting on the Tb³⁺ ion and obtain the expressions for these parameters as functions of three exchange-charge model parameters (G_s , G_σ , G_π) and the effective ligand charge (Z). The advantage of this approach, based on the exchange-charge model, is that it allows one to achieve a significant reduction of the number of parameters of the model from seven parameters (a_l^m and b_l^m) of the crystal field for the Tb³⁺ ion to only three parameters (G_s , G_σ , G_π) that characterize the exchange-charge contribution. Typically, the parameters G_s , G_σ , G_π are determined by simulating the observed Stark structure of the

Table 2. Numerical Values of the Crystal Field Parameters

	Crystal Field Parameters (cm ⁻¹)						
	a ₂ ⁰ /α	a ₄ ⁰ /β	a ₄ ⁴ /β	b ₄ ⁴ /β	a ₆ ⁰ /γ	a ₆ ⁴ /γ	b ₆ ⁴ /γ
point	51.8	-46.7	29.0	70.6	2.9	9.3	24.0
exchange	121.2	-584.7	368.4	882.4	76.8	247.1	643.0
total	173.0	-631.4	397.4	953.0	79.7	256.4	667.0

J-multiplet of a single lanthanide ion in the crystal field induced by its ligand surrounding. However, as already mentioned, the usual procedure of extracting the Stark structure of lanthanides from the optical spectra is not available for the Tb³⁺ complex under study. That is why we have applied the best-fit procedure for the simultaneous description of the magnetic susceptibility, paramagnetic shifts, and relaxation characteristics of the [Pc₂Tb]⁻TBA⁺ complexes and considered the parameters *G_s*, *G_σ*, *G_π* as fitting ones, keeping in mind that *G_s*, *G_σ*, *G_π* are positive.^{46,47} The simultaneous fit of the magnetic susceptibility, paramagnetic shifts, and relaxation times to the experimental data gave us the possibility to avoid superfluous approximating flexibility in the determination of the crystal field parameters.

The fitting procedure included the following stages. First, for the initial set of the parameters *G_s*, *G_σ*, *G_π* we compute the energies and the wave functions of the Stark levels, which arise from the splitting of the ground ⁷F₆-multiplet of the Tb³⁺ ion by the crystal field (eq 1). In the basis of the wave functions of the ground ⁷F₆ term of the Tb³⁺ ion, we then construct and diagonalize the matrix of the Hamiltonian:

$$H = H_{cf} + \mu_B \mathbf{H} g_J \mathbf{J} \quad (18)$$

where the second term is the operator of interaction of the Tb³⁺ ion with the external magnetic field *H*, μ_B is the Bohr magneton, *g_J* is the Lande factor for the ground multiplet ⁷F₆ of the Tb³⁺ ion (*g_J* = 3/2), and *J* = *L* + *S* is the total angular momentum of the Tb³⁺ ion (*L* = 3, *S* = 3, and *J* = 6). Next, using the eigenfunctions and eigenvalues of the Hamiltonian described by eq 18, the principal values χ_{αα} (α = *x, y, z*) of the magnetic susceptibility tensor and the magnetic susceptibility χ for the powder sample are calculated with the aid of the following formulas:

$$\chi_{\alpha\alpha} = N_A k T \frac{\partial^2}{\partial H_\alpha^2} [\ln Z(H_\alpha)]_{H_\alpha \rightarrow 0}$$

$$\chi = \frac{1}{3} (\chi_{xx} + \chi_{yy} + \chi_{zz}) \quad (19)$$

where

$$Z(H_\alpha) = \sum_i \exp \left[-\frac{E_i(H_\alpha)}{kT} \right] \quad (20)$$

is the partition function and *E_i*(*H_α*) are the energies of the Tb³⁺ ion in the external magnetic field.

In order to obtain a more reliable and complete description of the physical properties of the [Pc₂Tb]⁻TBA⁺ complex and to reduce the flexibility in the determination of the exchange-charge model parameters *G_s*, *G_σ*, *G_π* we also calculate the paramagnetic shifts. In ref 61, the paramagnetic shift Δδ for the [Pc₂Tb]⁻TBA⁺ complex was defined as the deviation of the chemical shift δ of a paramagnetic species from that of the diamagnetic [Pc₂Y]⁻TBA⁺ complex. Since the protons are separated from the lanthanide ions by at least four atoms, it is anticipated that the Fermi contact contribution to the

paramagnetic shift is much smaller than the magnetic dipolar contribution. The dipolar contribution in the ¹H NMR paramagnetic shift Δδ is determined as

$$\Delta\delta = \frac{\Delta\nu}{\nu} = \left(\frac{3 \cos^2 \theta - 1}{2R^3} \right) (\chi_{zz} - \chi) \quad (21)$$

where ν is the resonance frequency in the reference diamagnetic molecule, Δν is the change in the frequency in the paramagnetic molecule, θ is the azimuth angle, which takes on different values for the protons near and far from the center and referred to as α and β protons, respectively, *R* is the distance between the paramagnetic center and the proton to be considered. In our calculations, we used *R* and θ values estimated from the X-ray crystal structures of the [Pc₂Tb]⁻TBA⁺ compound.⁴⁵

3. RESULTS AND DISCUSSION

3.1. Magnetic Susceptibility. For the calculation of the cluster energy levels that determine the magnetic susceptibility, the ¹H NMR paramagnetic shifts, and the relaxation times, it is necessary to determine the charges of the ligands surrounding the Tb ion. Actually, to get accurate values of atomic charges, a calculation of the full electronic structure of the crystal is needed, which represents a separate problem. In our calculations, the numerical values of the ligand point charges have been identified approximately with the oxidation states and determined from the following considerations. Since the oxidation state of the Pc ligand is -2,⁶¹ the oxidation state of the each of four nitrogen ligands constituting the Pc ring was taken to be equal to -0.5. The best-fit parameters providing a satisfactory agreement between the calculated and experimental values of the magnetic susceptibility, ¹H NMR paramagnetic shifts, and relaxation times were found to be *G_s* = 6.2, *G_σ* = 38.2, *G_π* = 49.5. The obtained numerical values of the crystal field parameters are listed in Table 2. For each parameter, the contribution of the point and exchange charges is indicated. It is seen that the main contribution to the crystal field parameters comes from the exchange charge field. At first glance, this result appears to be unclear because for lanthanide ions the covalence effects are usually weak. On the other hand, the Tb³⁺ ion is placed between two π-conjugated planar ligands and the electronic density is mainly distributed among the N atoms within each of the two Pc rings. The latter probably leads to the dominance of the exchange-charge contribution.

The temperature dependences of the powder magnetic susceptibility and the principal values of the magnetic susceptibility tensor calculated with the best-fit parameters are shown in Figure 1. The most remarkable feature of the [Pc₂Tb]⁻TBA⁺ complex is the significant magnetic anisotropy exhibited by this system. At temperatures below 100 K, the components χ_{xx}*T* and χ_{yy}*T* are close to zero, while the component χ_{zz}*T* maintains a constant value of ~30 emu K mol⁻¹. With further temperature increases, the χ_{zz}*T* component slightly decreases, while the χ_{xx}*T* and χ_{yy}*T* components increase

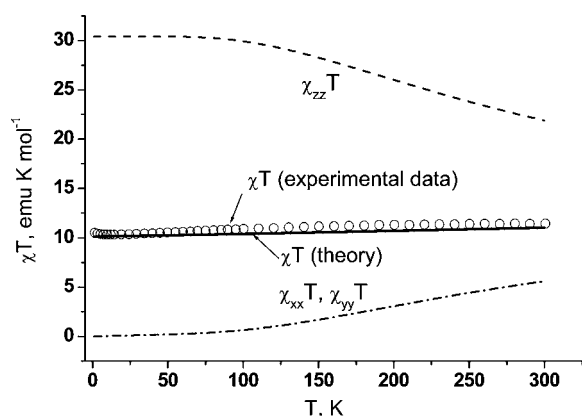


Figure 1. χT as a function of temperature for the $[Pc_2Tb]^-TBA^+$ cluster calculated with the set of the best-fit parameters $G_s = 6.2$, $G_\sigma = 38.2$, $G_\pi = 49.5$. The dashed line represents the $\chi_{zz}T$ component, the dash-dotted line represents $\chi_{xx}T$, $\chi_{yy}T$ components, the black solid line represents χT , and the circles denote experimental data.⁶¹ Agreement criteria: $\delta = \{(1/N)\sum_{i=1}^N [(\chi T)_i^{\text{theor}} - (\chi T)_i^{\text{exp}}]^2 / ((\chi T)_i^{\text{exp}})^2\}^{1/2} = 2.1\%$.

insignificantly. Thus, the difference $\Delta\chi T = \chi_{||}T - \chi_{\perp}T$ is large in a wide temperature range, and this observation is consistent with the experimental finding that the $[Pc_2Tb]^-TBA^+$ complex exhibits the ac susceptibility signal at temperatures up to 40 K.²⁹ It should be also noted that very good agreement is obtained between the observed⁶¹ and calculated χT values.

3.2. Barrier for Magnetization Reversal. The other manifestation of the strong axial magnetic anisotropy of the $[Pc_2Tb]^-TBA^+$ complex is the significant height of the barrier for magnetization reversal. In order to construct this barrier, we examine the low-lying part of the energy pattern of the $[Pc_2Tb]^-TBA^+$ complex in the absence of the external magnetic field calculated with the found set of the best-fit parameters. We find that the energy levels of the complex are nearly doubly degenerate. We then characterize each state ν of the cluster with the wave function $\psi_\nu = \sum_{j_z} C_{j_z}^{\nu} |j_z\rangle$ by the expectation value $\bar{J}_z = \langle \psi_\nu | \hat{J}_z | \psi_\nu \rangle$ of the total angular momentum projection of the complex. Figure 2 shows the low-lying energy levels of the Tb complex; for each level the corresponding \bar{J}_z value is indicated. The doubly degenerate ground level corresponds to $\hat{J}_z = \pm 6$, while, for the first excited doublet the value $\bar{J}_z = 0$. It is clearly seen that the energies of the first doublets with $\bar{J}_z = \pm 6$ and $\bar{J}_z = 0$ tend to decrease with enhance of \bar{J}_z . Thus, in this case, the barrier for magnetization reversal is formed only by two levels.

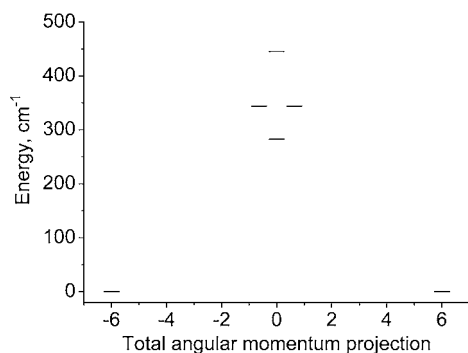


Figure 2. Energy levels of the single Tb^{3+} ion as functions of the total angular momentum projection \bar{J}_z calculated with $G_s = 6.2$, $G_\sigma = 38.2$, $G_\pi = 49.5$.

The height of the barrier is approximately equal to 282 cm^{-1} . This value differs significantly from that of 420 cm^{-1} obtained in ref 61 under assumption of the linear dependence of the crystal field parameters on the number of 4f electrons. It should be also mentioned that the barrier height discussed in the model suggested above is estimated in the static approximation based on the crystal field calculations of the energy spectrum of the terbium(III) ion and, therefore, it differs from that obtained in ref 40 from the analysis of the nuclear spin–lattice relaxation rates.

Finally, in Table 3, the coefficients characterizing the main contributions of the basis states $|J_z\rangle$ to the wave functions of the

Table 3. Squares ($|C_{j_z}^{\nu}|^2$) of the Coefficients Characterizing the Main Contributions of the Basis States $|J_z\rangle$ to the Wavefunctions of the Ground and First Excited States of the Tb^{3+} Ion

J_z		$ C_{j_z}^{\nu} ^2$
	Ground State	
6		1.0
	First Excited State	
-4		0.0117
0		0.9765
4		0.0117

ground and first excited levels of the $[Pc_2Tb]^-TBA^+$ complex are listed. Since the states of the complex are practically doubly degenerate, only the squares of the coefficients $|C_{j_z}^{\nu}|^2$ for one of the two wave functions corresponding to each level are given. From Table 3, it is seen that the ground state corresponds with $J_z = \pm 6$. The main contribution to the wave function of the first excited state comes from the component of the wave function complying with $J_z = 0$. All other contributions to this wave function are negligibly small, compared to this contribution.

3.3. Paramagnetic Shifts. Now, with the aid of eq 21, we perform the numerical evaluation of the paramagnetic shifts in the complex under examination. The distances and the azimuth angles for the α and β protons are $R_\alpha = 6.16 \text{ \AA}$ and $\theta_\alpha = 69.3^\circ$, and $R_\beta = 7.73 \text{ \AA}$ and $\theta_\beta = 69.8^\circ$,⁴⁵ respectively. With the aid of the calculated room-temperature $\chi T = 11.03 \text{ emu K mol}^{-1}$ and $\chi_{zz}T = 21.95 \text{ emu K mol}^{-1}$ for the paramagnetic shifts (see eq 21) of the α and β protons, we obtain the following: $\Delta\delta^{\text{calc}}(\alpha) = -80.3$, $\Delta\delta^{\text{calc}}(\beta) = -41.8$. These values are in a satisfactory agreement with those observed experimentally:⁶¹ $\Delta\delta^{\text{calc}}(\alpha) = -94.2$, $\Delta\delta^{\text{calc}}(\beta) = -48.7$.

3.4. Relaxation Characteristics of the $[Pc_2Tb]^-TBA^+$ Complex. For calculation of the relaxation characteristics of the complex under examination, the following simplifying assumptions have been accepted. First, the local symmetry of the Tb ion was supposed to differ insignificantly from that described by the point group D_{4d} . Second, an idealized model of the phonon spectrum with the Debye dispersion law (see eq 17) was employed. In order to justify the first assumption, the energy pattern of the $[Pc_2Tb]^-TBA^+$ complex was calculated, neglecting the rhombic distortion of the complex. In this case, the crystal field Hamiltonian described by eq 6 only contains the first three terms, and the energy pattern of the system consists of 7 levels, which correspond to the irreducible representations A_1 , (B_1, B_2) , E_1 , E_2 , and E_3 ⁶² of the D_{4d} point group (see Figure 3a). The energy gap between the ground state and the first excited state amounts to 300 cm^{-1} .

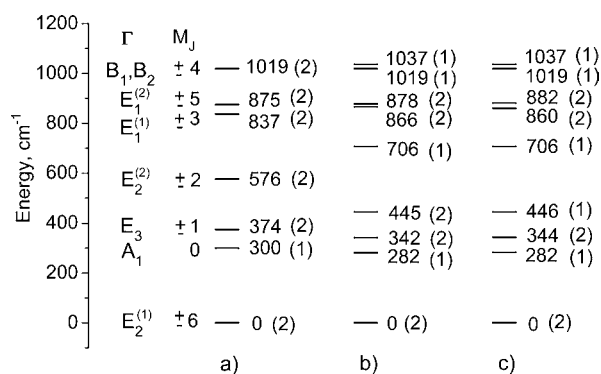


Figure 3. Energy pattern of the $[Pc_2Tb]^-TBA^+$ cluster calculated with the set of the best-fit parameters $G_s = 6.2$, $G_\sigma = 38.2$, $G_\pi = 49.5$: (a) in the case of D_{4d} symmetry; (b) with due account of the rhombic distortion in the second order of the perturbation theory; and (c) in the case of the real symmetry.

Considering the last four terms of the Hamiltonian described by eq 6 as a perturbation and calculating the corrections to the energy levels depicted in Figure 3a within the second-order approximation, we obtain the Stark structure of the multiplet 7F_6 shown in Figure 3b. Finally, the energy pattern calculated by diagonalization of the total Hamiltonian described by eq 6 is shown in Figure 3c. It is worth noting that the energies of the levels presented in Figures 3b and 3c practically coincide. This means that, to a great extent, the last four terms of the Hamiltonian described by eq 6 represent a small perturbation, which removes the degeneracy of the energy levels shown in Figure 3a. It is also worth noting that the energy gap between the ground state and the first excited Stark levels in the real symmetry differs from that in the idealized symmetry only by 8 cm^{-1} . The performed analysis of the Stark structure allows one to conclude that the symmetry of the complex can be described to a good approximation by the D_{4d} point group. In the subsequent calculations of the operators $V_{\mu\Gamma\gamma}(\kappa\eta)$ and coefficients $f_{\mu\Gamma\gamma}(\kappa\eta)$ for the average bond length R and the skew angle φ , we use the values of 2.44 \AA and 45° , respectively. At the same time, for the spherical angles θ_i characterizing the ligand positions, we retain the values given in Table 1.

The simplifications made allow us to take advantage of the group theory in the description of the relaxation characteristics of the $[Pc_2Tb]^-TBA^+$ complex. In order to calculate the probabilities of the transitions $W_{\tilde{\mu}\tilde{\Gamma}\tilde{\gamma} \rightarrow \mu\Gamma\gamma}$ given by eq 17, it is necessary to determine the symmetry of all possible vibrational modes of the system. For the idealized system of D_{4d} symmetry, the nearest ligand surrounding of the Tb^{3+} ion formed by eight N atoms possesses the following 18 active vibrational modes:

$$\Gamma = 2A_1, B_1, B_2, 2E_1, 3E_2, 2E_3 \quad (22)$$

Among them, 14 descend from 7 doubly degenerate representations, while the other 4 vibrational modes are nondegenerate and belong to the irreducible representations A_1, B_1, B_2 . For each of the vibrational modes, the corresponding symmetrized coordinates $Q_{\mu\Gamma\gamma}$, Van Vleck coefficients $f_{\mu\Gamma\gamma}(\kappa\eta)$, and vibronic operators $V_{\mu\Gamma\gamma}$ have been obtained. The analytical expressions for $Q_{\mu\Gamma\gamma}$ are listed in Appendix B, and the coefficients $f_{\mu\Gamma\gamma}(\kappa\eta)$ and the operators $V_{\mu\Gamma\gamma}$ are given in the Supporting Information. It should be highlighted that the vibrational operators $V_{\mu\Gamma\gamma}$ (see the Supporting Information) take into account both the contributions from the point and exchange charges.

Now we are in the position to evaluate the temperature dependence of the relaxation time for magnetization from the solution of the set of master equations. For each state $|\mu\Gamma\gamma\rangle$ depicted in Figure 3a, we take into account all transitions populating and depopulating this state. Since the levels corresponding to the irreducible representations (B_1, B_2), E_1, E_2 , and E_3 are doubly degenerate, while the A_1 level is nondegenerate in the process of relaxation there are involved 13 states. The probabilities of the transitions between all mentioned states have been calculated with the aid of expression 17. The system of the master equations for the populations $n_{\mu\Gamma\gamma}$ of the 13 states of the Tb^{3+} complex (Figure 3a) appears as follows:

$$\frac{\partial n_{\tilde{\mu}\tilde{\Gamma}\tilde{\gamma}}}{\partial t} = -n_{\tilde{\mu}\tilde{\Gamma}\tilde{\gamma}} \sum_{\substack{\Gamma, \gamma, \mu \\ \gamma \neq \tilde{\gamma}}} W_{\tilde{\mu}\tilde{\Gamma}\tilde{\gamma} \rightarrow \mu\Gamma\gamma} + \sum_{\substack{\Gamma, \gamma, \mu \\ \gamma \neq \tilde{\gamma}}} W_{\mu\Gamma\gamma \rightarrow \tilde{\mu}\tilde{\Gamma}\tilde{\gamma}} n_{\mu\Gamma\gamma} \quad (23)$$

Here, $W_{\tilde{\mu}\tilde{\Gamma}\tilde{\gamma} \rightarrow \mu\Gamma\gamma}$ is the probability of the transition between the electronic states $|\tilde{\mu}\tilde{\Gamma}\tilde{\gamma}\rangle$ and $|\mu\Gamma\gamma\rangle$, and the symbols $\tilde{\mu}$ and μ have been introduced to enumerate the repeating electronic representations. The set of master eqs 23 can be presented in vector form:

$$\dot{\mathbf{n}}(t) = \tilde{W}\mathbf{n}(t) \quad (24)$$

where \tilde{W} is the rate matrix and the elements of the vector $\mathbf{n}(t)$ are the populations of the states $|\tilde{\mu}\tilde{\Gamma}\tilde{\gamma}\rangle$. The relaxation time then is obtained by numerical diagonalization of the rate matrix. Denoting the eigenvalues of the rate matrix by w_i (i runs over 13 states), we find that the dominant relaxation time of the system is given by

$$\tau = \max_i \left\{ -\frac{1}{\text{Re}(w_i)} \right\} \quad (25)$$

In calculations of the relaxation time, for the crystal density the value $\rho = 1.38 \text{ g/cm}^3$ (from ref 45 has been used). Our fit of the sound velocity gives $v_{\text{eff}} = 3.1 \times 10^5 \text{ cm/s}$. This value is in satisfactory agreement with that obtained for a Tb^{3+} complex in ref 63. As already mentioned in previous sections for the parameters of the exchange charge model, the same values as those used in calculations of the magnetic susceptibility and paramagnetic shifts have been taken: $G_s = 6.2$, $G_\sigma = 38.2$, $G_\pi = 49.5$. The calculated and experimental values of the relaxation times at different temperatures are listed in Table 4.

The best agreement between theoretical and experimentally observed relaxation times is observed at $T = 40 \text{ K}$. In this case, the theoretical value of the relaxation time ($\tau_{\text{theor}} = 1.52 \times 10^{-4} \text{ s}$) is only 5.6% less than the experimental one ($\tau_{\text{exp}} = 1.61 \times 10^{-4} \text{ s}$). At temperatures of $T = 34 \text{ K}$ and $T = 27 \text{ K}$, the differences between the experimental and calculated values of

Table 4. Calculated and Experimental³⁰ Values of the Relaxation Times (τ) of the $[Pc_2Tb]^-TBA^+$ Cluster

temperature, T (K)	Relaxation Time, τ	
	theory	experimental data ^a
14	$9.7 \times 10^5 \text{ s}$	0.157 s
27	$3.20 \times 10^{-2} \text{ s}$	$1.58 \times 10^{-2} \text{ s}$
34	$1.11 \times 10^{-3} \text{ s}$	$1.57 \times 10^{-3} \text{ s}$
40	$1.52 \times 10^{-4} \text{ s}$	$1.61 \times 10^{-4} \text{ s}$

^aData taken from ref 30.

the relaxation times are more significant, but the experimental and theoretical values still are of the same order of magnitude. Finally, at $T = 14$ K, the calculated value of the relaxation time significantly exceeds the corresponding experimental value. Probably, the agreement between the theoretical and experimental values of the relaxation times at low temperatures can be achieved by taking into account the higher-order Orbach and Raman relaxation processes, as well as the phonon-assisted tunneling induced by the rhombic part of the crystal field Hamiltonian and hyperfine interactions. These are problems that we will address in the future.

4. CONCLUDING REMARKS

The results obtained can be summarized as follows. A general scheme for the microscopic calculation of the parameters of the ligand field for lanthanide ions was elaborated. The covalence effects and the real symmetry of the crystal surrounding of the Tb ion in $[Pc_2Tb]^-TBA^+$ have been taken into account. The energies and wave functions of the Stark levels arising from the splitting of the ground 7F_6 multiplet of the Tb^{3+} ion in the ligand field have been computed. On this basis, the principal values of the magnetic susceptibility tensor have been found. A reasonable agreement between the calculated and observed magnetic susceptibility⁶¹ has been obtained. In the tetragonal crystal field induced by nitrogen ligands, the energies of low-lying Stark levels of the Tb^{3+} ion increase as the mean value of the z-projection of the total angular momentum decreases, which is a situation that leads to a barrier for the reversal of magnetization. Thus, the model explains the discovered single-molecule magnet (SMM) behavior of the $[Pc_2Tb]^-TBA^+$ complex arising from the strong single-ion anisotropy associated with the unquenched orbital angular momenta of the lanthanide ions.

The Hamiltonian of the electron–phonon interaction for the Tb^{3+} ion in $[Pc_2Tb]^-TBA^+$ was obtained. The direct one-phonon transitions between the low-lying Stark levels of the Tb ion have been assumed to be responsible for magnetization relaxation. The calculated relaxation times in the temperature range of 27–40 K are in very good agreement with the experimental ones. In order to explain the observed temperature dependence of the relaxation time in a wide temperature range in the future, we will estimate the contributions of relaxation processes facilitated by quadratic terms of electron–phonon interaction and phonon-assisted tunneling induced by hyperfine interactions and deviations of the crystal field symmetry from the axial one.

At the same time, the unified microscopic approach developed in the present paper provides a reasonable qualitative and quantitative explanation of the comprehensive experimental data⁶¹ on the magnetic susceptibility, relaxation characteristics, and paramagnetic shifts of the $[Pc_2Tb]^-TBA^+$ SMM.

APPENDIX A. CRYSTAL FIELD HAMILTONIAN

In order to simplify the calculation of the energies and wave functions of the Stark levels arising from the splitting of the ground 7F_6 multiplet of the Tb^{3+} ion by the crystal field, we pass to the equivalent operators.⁵⁸ With this objective, at the first stage, we introduce the tesseral harmonics:⁶⁴

$$Z_{l,0} = Y_{l,0}$$

$$Z_{l,m}^c = \frac{1}{\sqrt{2}}(Y_{l,m} + (-1)^m Y_{l,-m})$$

$$Z_{l,m}^s = \frac{i}{\sqrt{2}}(Y_{l,-m} - (-1)^m Y_{l,m}) \quad (A1)$$

which are determined as follows:

$$Z_{l,0} = \gamma_{l,0} V_l^0$$

$$Z_{l,m}^c = \frac{1}{\sqrt{2}} \gamma_{l,m} V_l^m$$

$$Z_{l,m}^s = \frac{i}{\sqrt{2}} \gamma_{l,m} W_l^m \quad (A2)$$

Here, V_l^m and W_l^m are homogeneous polynomials of Cartesian coordinates, and $\gamma_{l,0}$ and $\gamma_{l,m}$ are numerical coefficients quoted in Table A1.

Table A1. Coefficients $\gamma_{l,m}$

l	2	2	2	4	4	4	4	4
m	0	1	2	0	1	2	3	4
$\gamma_{l,m}$	$\frac{\sqrt{5}}{4\sqrt{\pi}}$	$\frac{1}{2\sqrt{6}}$	$\frac{1}{\sqrt{6}}$	$\frac{3}{16\sqrt{\pi}}$	$\frac{1}{4\sqrt{5}}$	$\frac{1}{2\sqrt{10}}$	$\frac{1}{4\sqrt{35}}$	$\frac{1}{\sqrt{70}}$
l	6	6	6	6	6	6	6	6
m	0	1	2	3	4	5	6	6
$\gamma_{l,m}$	$\frac{\sqrt{13}}{32\sqrt{\pi}}$	$\frac{1}{2\sqrt{42}}$	$\frac{1}{\sqrt{105}}$	$\frac{1}{2\sqrt{105}}$	$\frac{1}{3\sqrt{14}}$	$\frac{1}{6\sqrt{77}}$	$\frac{1}{\sqrt{231}}$	

The polynomials V_l^m and W_l^m correspond to equivalent operators O_l^m and Q_l^m , which possess the same transformational properties.^{58,65} This means that, within the set of functions belonging to the same total angular momentum J , the following relation can be written:

$$\langle J, M_J | \sum_i V_l^m(\mathbf{r}_i) | J, M_J' \rangle = \langle J || \xi_l || J \rangle \langle J, M_J | O_l^m | J, M_J' \rangle \quad (A3)$$

where the Stevens constant $\langle J || \xi_l || J \rangle$ depends on the electronic structure of the lanthanide ion as well as on the quantum numbers L , S , and J characterizing the LSJ multiplet of this ion. The commonly accepted notations for the Stevens constants are $\langle J || \xi_2 || J \rangle = \alpha$, $\langle J || \xi_4 || J \rangle = \beta$, $\langle J || \xi_6 || J \rangle = \gamma$. The explicit forms of the equivalent operators are given in ref 66. The matrix elements of operators O_l^m in the $|J, M_J\rangle$ basis are tabulated and can be found in a series of monographs and articles (see, for instance, ref 66). A simple relationship between the matrix elements of the operators O_l^m and Q_l^m takes place:

$$\langle J, M_J \pm ml | Q_l^m | J, M_J \rangle = \pm i \langle J, M_J \pm ml | O_l^m | J, M_J \rangle \quad (A4)$$

The operators O_l^m and Q_l^m are connected with combinations of the spherical harmonics in the following way:

$$O_{l,0} = \frac{1}{\langle J || \xi || J \rangle \gamma_{l,0}} Y_{l,0}(\vartheta, \varphi) \quad (l = 2, 4, 6)$$

$$O_{l,m} = \frac{1}{\langle J || \xi || J \rangle \gamma_{l,m}} (Y_{l,-m}(\vartheta, \varphi) - Y_{l,m}(\vartheta, \varphi))$$

$$(l = 2, 4, 6; m = 1, 2, \dots, l)$$

$$Q_{l,m} = \frac{i}{\langle J || \xi || J \rangle \gamma_{l,m}} (Y_{l,-m}(\vartheta, \varphi) + Y_{l,m}(\vartheta, \varphi))$$

$$(l = 2, 4, 6; m = 1, 2, \dots, l) \quad (\text{A5})$$

Calculating the overlap integrals and substituting the radia R_α and angles ϑ_ω φ_α into eqs 3 and 4 and then, passing to the equivalent operators, one obtains the following expressions for the parameters a_i^m and b_i^m :

$$a_2^0 = \left[5.97G_p + 2.80G_\pi + 2.75G_s + 687.95(1 - \sigma_2)Z \right] \times \left(\frac{1}{4} \right) \sqrt{\frac{5}{\pi}} \alpha$$

$$a_4^0 = \left[-119.65G_p - 12.45G_\pi - 54.96G_s - 873.08(1 - \sigma_4)Z \right] \left(\frac{3}{16\sqrt{\pi}} \right) \beta$$

$$a_4^4 = \left[9.0G_p + 0.95G_\pi + 4.16G_s + 64.91(1 - \sigma_4)Z \right] \left(\frac{3}{8} \right) \times \sqrt{\frac{35}{2\pi}} \beta$$

$$b_4^4 = \left[21.59G_p + 2.24G_\pi + 9.90G_s + 157.80(1 - \sigma_4)Z \right] \times \left(\frac{3}{8} \right) \sqrt{\frac{35}{2\pi}} \beta$$

$$a_6^0 = \left[67.55G_p - 31.64G_\pi + 31.03G_s + 87.50(1 - \sigma_6)Z \right] \times \left(\frac{1}{32} \right) \sqrt{\frac{13}{\pi}} \gamma$$

$$a_6^4 = \left[19.64G_p - 9.31G_\pi + 9.10G_s + 25.32(1 - \sigma_6)Z \right] \times \left(\frac{3}{16} \right) \sqrt{\frac{91}{2\pi}} \gamma$$

$$b_6^4 = \left[50.29G_p - 23.51G_\pi + 23.07G_s + 65.19(1 - \sigma_6)Z \right] \times \left(\frac{3}{16} \right) \sqrt{\frac{91}{2\pi}} \gamma \quad (\text{A6})$$

■ APPENDIX B. SYMMETRICAL DISPLACEMENTS OF THE COMPLEX

$$Q_{A_1}^{(1)} = 0.26257(x_1 - x_3 + x_5 - x_7 + y_2 - y_4 + y_6 - y_8) + 0.10876(x_2 - x_4 - x_6 + x_8 - y_1 + y_3 + y_5 - y_7) + 0.21030(-z_1 - z_2 - z_3 - z_4 + z_5 + z_6 + z_7 + z_8) \quad (\text{B1})$$

$$Q_{A_1}^{(2)} = 0.19429(x_1 - x_3 + x_5 - x_7 + y_2 - y_4 + y_6 - y_8) + 0.08047(x_2 - x_4 - x_6 + x_8 - y_1 + y_3 + y_5 - y_7) + 0.28421(z_1 + z_2 + z_3 + z_4 - z_5 - z_6 - z_7 - z_8) \quad (\text{B2})$$

$$Q_{B_1} = \frac{1}{4} \sqrt{1 - \frac{1}{\sqrt{2}}} (x_1 - x_3 + x_5 - x_7 + y_2 - y_4 + y_6 - y_8) + \frac{1}{4} \sqrt{1 + \frac{1}{\sqrt{2}}} (-x_2 + x_4 + x_6 - x_8 + y_1 - y_3 - y_5 + y_7) \quad (\text{B3})$$

$$Q_{B_2} = \frac{1}{4} \sqrt{1 + \frac{1}{\sqrt{2}}} (-x_1 + x_3 + x_5 - x_7 - y_2 + y_4 + y_6 - y_8) + \frac{1}{4} \sqrt{1 - \frac{1}{\sqrt{2}}} (-x_2 + x_4 - x_6 + x_8 + y_1 - y_3 + y_5 - y_7) \quad (\text{B4})$$

$$Q_{E_{1,1}}^{(1)} = \frac{1}{4} (-x_5 + x_6 - x_7 + x_8 + y_1 - y_2 + y_3 - y_4) + \frac{i}{4} (x_1 - x_2 + x_3 - x_4 + y_5 - y_6 + y_7 - y_8) \quad (\text{B5})$$

$$Q_{E_{1,2}}^{(1)} = \frac{1}{4} (x_1 - x_2 + x_3 - x_4 + y_5 - y_6 + y_7 - y_8) + \frac{i}{4} (-x_5 + x_6 - x_7 + x_8 + y_1 - y_2 + y_3 - y_4) \quad (\text{B6})$$

$$Q_{E_{1,1}}^{(2)} = \frac{1}{4} [-z_5 - z_6 + z_7 + z_8 + i(z_5 - z_6 - z_7 + z_8)] + \frac{1}{2\sqrt{2}} [z_2 - z_4 + i(-z_1 + z_3)] \quad (\text{B7})$$

$$Q_{E_{1,2}}^{(2)} = \frac{1}{4} [-z_1 + z_2 + z_3 - z_4 + i(z_1 + z_2 - z_3 - z_4)] + \frac{1}{2\sqrt{2}} [-z_6 + z_8 + i(-z_5 + z_7)] \quad (\text{B8})$$

$$Q_{E_{2,1}}^{(1)} = \frac{1}{2\sqrt{2}} (-x_5 + x_7 + y_6 - y_8) + \frac{i}{4} (x_1 - x_2 - x_3 + x_4 - y_5 - y_6 + y_7 + y_8) \quad (\text{B9})$$

$$Q_{E_{2,2}}^{(1)} = \frac{1}{2\sqrt{2}} (-x_1 + x_3 + y_2 - y_4) + \frac{i}{4} (x_5 + x_6 - x_7 - x_8 + y_5 - y_6 - y_7 + y_8) \quad (\text{B10})$$

$$Q_{E_{2,1}}^{(2)} = \frac{1}{2\sqrt{2}} (x_6 - x_8 + y_6 - y_8) + \frac{i}{4} (-x_1 - x_2 + x_3 + x_4 - y_1 + y_2 + y_3 - y_4) \quad (\text{B11})$$

$$Q_{E_{2,2}}^{(2)} = \frac{1}{2\sqrt{2}} (-x_2 + x_4 - y_1 + y_3) + \frac{i}{4} (-x_5 + x_6 + x_7 - x_8 + y_5 + y_6 - y_7 - y_8) \quad (\text{B12})$$

$$Q_{E_{2,1}}^{(3)} = \frac{1}{2\sqrt{2}} [-z_5 + z_6 - z_7 + z_8 + i(-z_1 + z_2 - z_3 + z_4)] \quad (\text{B13})$$

$$Q_{E_{2,2}}^{(3)} = \frac{1}{2\sqrt{2}}[z_1 - z_2 + z_3 - z_4 + i(z_5 - z_6 + z_7 - z_8)] \quad (\text{B14})$$

$$Q_{E_{3,1}}^{(1)} = \frac{1}{2\sqrt{2}}[-x_5 - x_7 + i(-y_5 - y_7)] \\ + \frac{1}{4\sqrt{2}}[x_1 + x_2 + x_3 + x_4 + i(-x_1 + x_2 - x_3 + x_4)] \\ + \frac{1}{4\sqrt{2}}[-y_1 + y_2 - y_3 + y_4 + i(y_1 + y_2 + y_3 + y_4)] \quad (\text{B15})$$

$$Q_{E_{3,2}}^{(1)} = \frac{1}{2\sqrt{2}}[x_1 + x_3 + i(-y_2 - y_4)] \\ + \frac{1}{4\sqrt{2}}[-x_5 - x_6 - x_7 - x_8 + i(x_5 - x_6 + x_7 - x_8)] \\ + \frac{1}{4\sqrt{2}}[-y_5 + y_6 - y_7 + y_8 + i(y_5 + y_6 + y_7 + y_8)] \quad (\text{B16})$$

$$Q_{E_{3,1}}^{(2)} = \frac{1}{4}[z_5 + z_6 - z_7 - z_8 + i(-z_5 + z_6 + z_7 - z_8)] \\ + \frac{1}{2\sqrt{2}}[z_2 - z_4 + i(-z_1 + z_3)] \quad (\text{B17})$$

$$Q_{E_{3,2}}^{(2)} = \frac{1}{4}[z_1 - z_2 - z_3 + z_4 + i(-z_1 - z_2 + z_3 + z_4)] \\ + \frac{1}{2\sqrt{2}}[-z_6 + z_8 + i(-z_5 + z_7)] \quad (\text{B18})$$

where x_i , y_i , and z_i are Cartesian displacements of the i th ligand.

■ ASSOCIATED CONTENT

■ Supporting Information

Information pertaining to Van Vleck coefficients and vibronic operators is provided as Supporting Information. This material is available free of charge via the Internet at <http://pubs.acs.org>.

■ AUTHOR INFORMATION

Corresponding Author

*E-mail: klokishner@yahoo.com.

Notes

The authors declare no competing financial interest.

†Deceased.

■ ACKNOWLEDGMENTS

Financial support of Swiss National Science Foundation (Grant No. IZ73Z0-128078/1) and Supreme Council for Science and Technological Development of Moldova is highly appreciated.

■ REFERENCES

- Gatteschi, D.; Sessoli, R. *Angew. Chem., Int. Ed.* **2003**, *42*, 268.
- Bogani, L.; Wernsdorfer, W. *Nat. Mater.* **2008**, *7*, 179–186.
- Leuenberger, M. N.; Loss, D. *Nature* **2001**, *410*, 789.
- Sessoli, R.; Tsai, H.-L.; Schake, A. R.; Wang, S.; Vincent, J. B.; Folting, K.; Gatteschi, D.; Christou, G.; Hendrickson, D. N. *J. Am. Chem. Soc.* **1993**, *115*, 1804.
- Sessoli, R.; Matteschi, D.; Caneschi, A.; Novak, M. A. *Nature* **1993**, *365*, 141.
- Thomas, L.; Lioni, F.; Ballou, R.; Gatteschi, D.; Sessoli, R.; Barbara, B. *Nature* **1996**, *383*, 145.
- Friedman, J. R.; Sarachik, M. P. *Phys. Rev. Lett.* **1996**, *76*, 3830.
- Eppley, H. J.; Tsai, H.-L.; de Vries, N.; Folting, K.; Christou, G.; Hendrickson, D. N. *J. Am. Chem. Soc.* **1995**, *117*, 301.

(9) Aubin, S. M. J.; Spagna, S.; Eppley, H. J.; Sager, R. E.; Christou, G.; Hendrickson, D. N. *Chem. Commun.* **1998**, *7*, 803.

(10) Aubin, S. M. J.; Sun, Z.; Pardi, L.; Krzystek, J.; Folting, K.; Brunel, L.-C.; Rheingold, A. L.; Christou, G.; Hendrickson, D. N. *Inorg. Chem.* **1999**, *38*, 5329.

(11) Soler, M.; Chandra, S. K.; Ruiz, D.; Davidson, E. R.; Hendrickson, D. N.; Christou, G. *Chem. Commun.* **2000**, *24*, 2417.

(12) Boskovic, C.; Pink, M.; Huffman, J. C.; Hendrickson, D. N.; Christou, G. *J. Am. Chem. Soc.* **2001**, *123*, 9914.

(13) Aubin, S. M. J.; Wemple, M. W.; Adams, D. M.; Tsai, H. L.; Christou, G.; Hendrickson, D. N. *J. Am. Chem. Soc.* **1996**, *118*, 7746.

(14) Aubin, S. M. J.; Dilley, N. R.; Pardi, L.; Krzystek, J.; Wemple, M. W.; Brunel, L. C.; Maple, M. B.; Christou, G.; Hendrickson, D. N. *J. Am. Chem. Soc.* **1998**, *120*, 4991.

(15) Andres, H.; Basler, R.; Güdel, H.-U.; Aromi, G.; Christou, G.; Buttner, H.; Ruffle, B. *J. Am. Chem. Soc.* **2000**, *122*, 12469.

(16) Castro, S. L.; Sun, Z.; Grant, C. M.; Bollinger, J. C.; Hendrickson, D. N.; Christou, G. *J. Am. Chem. Soc.* **1998**, *120*, 2365.

(17) Sangregorio, C.; Ohm, T.; Paulsen, C.; Sessoli, R.; Matteschi, D. *Phys. Rev. Lett.* **1997**, *78*, 4645.

(18) Waldmann, O. *Inorg. Chem.* **2007**, *46*, 10035.

(19) Choi, H. J.; Sokol, J. J.; Long, J. R. *Inorg. Chem.* **2004**, *43*, 1606.

(20) Berlinguette, C. P.; Vaughn, D.; Cañada-Vilalta, C.; Galán-Mascarós, J.-R.; Dunbar, K. R. *Angew. Chem., Int. Ed.* **2003**, *42*, 1523.

(21) Wang, S.; Zuo, J. L.; Zhou, H. C.; Choi, H. J.; Ke, Y.; Long, J. R. *Angew. Chem., Int. Ed.* **2004**, *43*, 5940.

(22) Schelter, E. J.; Prosvirin, A. V.; Dunbar, K. R. *J. Am. Chem. Soc.* **2004**, *126*, 15004.

(23) Pali, A. V.; Ostrovsky, S. M.; Klokishner, S. I.; Tsukerblat, B. S.; Galán-Mascarós, J. R.; Berlinguette, C. P.; Dunbar, K. R. *J. Am. Chem. Soc.* **2004**, *126*, 16860.

(24) Tsukerblat, B. S.; Pali, A. V.; Ostrovsky, S. M.; Kunitsky, S. V.; Klokishner, S. I.; Dunbar, K. R. *J. Chem. Theory Comput.* **2005**, *1*, 668.

(25) Pali, A. V.; Ostrovsky, S. M.; Klokishner, S. I.; Tsukerblat, B. S.; Dunbar, K. R. *Chem. Phys. Chem.* **2006**, *7*, 871.

(26) Ostrovsky, S. M.; Klokishner, S. I.; Pali, A. V.; Dunbar, K. R. *J. Mol. Struct.* **2007**, *838*, 138.

(27) Klokishner, S. I.; Ostrovsky, S. M.; Pali, A. V.; Dunbar, K. R. *J. Mol. Struct.* **2007**, *838*, 144.

(28) Pali, A. V.; Ostrovsky, S. M.; Klokishner, S. I.; Tsukerblat, B. S.; Schelter, E. J.; Prosvirin, A. V.; Dunbar, K. R. *Inorg. Chim. Acta* **2007**, *360*, 3915.

(29) Ishikawa, N.; Sugita, M.; Ishikawa, T.; Koshihara, S.; Kaisu, Y. *J. Am. Chem. Soc.* **2003**, *125*, 8694.

(30) Ishikawa, N.; Sugita, M.; Ishikawa, T.; Koshihara, S.; Kaisu, Y. *J. Phys. Chem. B* **2004**, *108*, 11265.

(31) Ishikawa, N.; Sugita, M.; Wernsdorfer, W. *J. Am. Chem. Soc.* **2005**, *127*, 3650.

(32) Ishikawa, N.; Sugita, M.; Wernsdorfer, W. *Angew. Chem., Int. Ed.* **2005**, *44*, 2931.

(33) Al-Damen, M. A.; Clemente-Juan, J. M.; Coronado, E.; Martí-Gastaldo, C.; Gaita-Ariño, A. *J. Am. Chem. Soc.* **2008**, *130*, 8874.

(34) Al-Damen, M. A.; Cardona-Serra, S.; Clemente-Juan, J. M.; Coronado, E.; Gaita-Ariño, A.; Martí-Gastaldo, C.; Luis, F.; Montero, O. *Inorg. Chem.* **2009**, *48*, 3467.

(35) Kyatskaya, S.; Galan Mascaros, J. R.; Bogani, L.; Hennrich, F.; Kappes, M.; Wernsdorfer, W.; Ruben, M. *J. Am. Chem. Soc.* **2009**, *131*, 15143.

(36) Urdampilletta, M.; Klyatskaya, S.; Cleuziou, J.-P.; Ruben, M.; Wernsdorfer, W. *Nat. Mater.* **2011**, *10*, 502.

(37) Vincent, R.; Klyatskaya, S.; Ruben, M.; Wernsdorfer, W.; Balestro, F. *Nature* **2012**, *488*, 357.

(38) Ishikawa, N.; Iino, T.; Kaizu, Y. *J. Phys. Chem. A* **2002**, *106*, 9543.

(39) Ishikawa, N. *J. Phys. Chem. A* **2003**, *107*, 5831.

(40) Branzoli, F.; Carretta, P.; Filibian, M.; Zopellaro, G.; Graf, M. J.; Galan-Mascaros, J. R.; Fuhr, O.; Brink, S.; Ruben, M. *J. Am. Chem. Soc.* **2009**, *131*, 4387.

- (41) Andriesh, I. S.; Gamurar, V. Ya.; Vylegzhanin, D. N.; Kaminskii, A. A.; Klokishner, S. I.; Perlin, Yu. E. *Sov. Phys.–Solid State* **1973**, *14*, 2550.
- (42) Andriesh, I. S.; Gamurar, V. Ya.; Vylegzhanin, D. N.; Kaminskii, A. A.; Klokishner, S. I.; Perlin, Yu. E. *Sov. J. Quantum Electron.* **1975**, *5*, 162.
- (43) Blaja, M. G.; Vylegzhanin, D. N.; Kaminskii, A. A.; Klokishner, S. I.; Perlin, Yu. E. *Bull. Acad. Sci. USSR; Phys. Ser.* **1976**, *40*, 69.
- (44) Perlin, Yu. E.; Kaminskii, A. A.; Klokishner, S. I.; Enakii, V. N.; Bagdasarov, Kh. S.; Bogomolova, G. A.; Vylegzhanin, D. N. *Cryst. Phys. Status Solidi (A)* **1977**, *40*, 643.
- (45) Koike, N.; Uekusa, H.; Ohashi, Y.; Harnood, C.; Kitamura, F.; Ohsaka, T.; Tokuda, K. *Inorg. Chem.* **1996**, *35*, 5798.
- (46) Malkin, B. Z. Crystal field and electron–phonon interaction in rare earth ionic paramagnets. In *Spectroscopy of Solids Containing Rare-Earth Ions*; Kaplyanskii, A. A.; Macfarlane, R. M., Ed.; North-Holland: Amsterdam, 1987; Vol. 13.
- (47) Popova, M. N.; Chukalina, E. P.; Malkin, B. Z.; Saikin, S. K. *Phys. Rev. B* **2000**, *61*, 7421.
- (48) Klokishner, S.; Melsheimer, J.; Jentoft, F. S.; Schlögl, R. *Phys. Chem. Chem. Phys.* **2004**, *6*, 2066.
- (49) Klokishner, S. I.; Tsukerblat, B. S.; Reu, O. S.; Pali, A. V.; Ostrovsky, S. M. *Chem. Phys.* **2005**, *316*, 83.
- (50) Klokishner, S. I.; Tsukerblat, B. S.; Reu, O. S.; Pali, A. V.; Ostrovsky, S. M. *Opt. Mater.* **2005**, *27*, 1445.
- (51) Klokishner, S. I.; Reu, O. S.; Ostrovsky, S. M.; Pali, A. V.; Kulyuk, L. L.; Tsukerblat, B. S.; Towe, E. J. *Mol. Struct.* **2007**, *838*, 133.
- (52) Klokishner, S. I.; Ostrovsky, S. M.; Reu, O. S.; Pali, A. V.; Tregenna-Piggott, P. L. W.; Nannestad, T. B.; Bendix, J.; Mutka, H. J. *Phys. Chem. C* **2009**, *113*, 8573.
- (53) Klokishner, S. I.; Reu, O.; Chan-Thaw, C. E.; Jentoft, F. C.; Schlögl, R. *J. Phys. Chem. A* **2011**, *115*, 8100.
- (54) Klokishner, S.; Behrens, M.; Reu, O.; Tzolova-Möüller, G.; Girgsdies, F.; Trunschke, A.; Schlögl, R. *J. Phys. Chem. A* **2011**, *115*, 9954.
- (55) Edvardson, S.; Klintonberg, M. J. *Alloys Compd.* **1998**, *275–277*, 230.
- (56) Freeman, A. J.; Watson, R. E. *Phys. Rev.* **1962**, *127*, 2058.
- (57) Clementi, E.; Mclean, A. D. *Phys. Rev.* **1964**, *133*, A419.
- (58) Stevens, K. W. H. *Proc. Phys. Soc. A* **1952**, *65*, 209.
- (59) Taylor, K. N. R.; Darby, M. I. *Physics of Rare Earth Solids*; Chapman and Hall, Ltd.: London, 1972.
- (60) Tsukerblat, B. S.; Perlin, Yu. E. *Effects of Electron–Vibrational Interaction in the Optical Spectra of Paramagnetic Impurity Ions*; Stiinta: Kishinev, Moldova, 1974.
- (61) Ishikawa, N.; Sugita, M.; Okubo, T.; Tanaka, N.; Iino, T.; Kaizu, Y. *Inorg. Chem.* **2003**, *42*, 2440.
- (62) Altmann, S. L.; Herzig, P. *Point-Group Theory Tables* Clarendon Press: Oxford, U.K., 1994.
- (63) Papagelis, K.; Ves, S. J. *Appl. Phys.* **2003**, *94*, 6491.
- (64) Hutchings, M. T. *Solid State Phys.* **1964**, *16*, 227.
- (65) Bleaney, B.; Stevens, K. W. H. *Rep. Prog. Phys.* **1953**, *16*, 108.
- (66) Abragam, A.; Bleaney, B. *Electron Paramagnetic Resonance of Transition Ions*; Clarendon Press: Oxford, U.K., 1970.